Identification and Mitigation of Anomalous Signals in CMS Hadronic Calorimeter



2012 J. Phys.: Conf. Ser. 404 012044

(http://iopscience.iop.org/1742-6596/404/1/012044)

Journal of Physics: Conference Series **404** (2012) 012044 doi:10.1088/1742-6596/404/1/012044

# Identification and Mitigation of Anomalous Signals in CMS Hadronic Calorimeter

**Artur Apresyan**

California Institute of Technology, Pasadena, California 91106
ON BEHALF OF THE CMS COLLABORATION

E-mail: apresyan@cern.ch

**Abstract.** The CMS HCAL detector occasionally records anomalous large energy signals that correspond to particles hitting the transducers. Anomalous signals in HCAL can also be produced by rare random discharges of the readout detectors. We present a summary of various sources of anomalous signals, the algorithms developed to identify them, and the performance of these algorithms in the CMS collision data.

## 1. The CMS hadronic calorimeter

The barrel and endcap hadronic calorimeter (HCAL) subdetectors of CMS detector [1, 2] completely surround the electromagnetic calorimeter (ECAL), and are immersed within the 3.8 T magnetic field of the solenoid. The barrel (HB) extends out to $|\eta| = 1.4$, and HE covers the overlapping range $1.3 < |\eta| < 3.0$. The forward calorimeters extend the pseudorapidity coverage from $|\eta| = 2.9$ to $|\eta| = 5$. The thickness of the HCAL sub-detectors varies from 7-11 $\lambda_{\mathrm{I}}$, depending on $|\eta|$.

In HB and HE the active plastic scintillator tiles are interspersed between the stainless steel and brass absorber plates [3, 4, 5]. The front-end electronics of each wedge (72 channels) are housed in an enclosure referred to as a read-out box (RBX). Each RBX contains four hybrid photodiodes (HPD) [6] which register signals from eighteen towers at a fixed $\phi$ angle. The HF is made of steel absorbers and embedded quartz fibers, which provide a fast collection of Čherenkov light. Two types of quartz fibers are used: "long" fibers span the length of HF, and "short" fibers begin 22 cm into the detector. The differing fiber lengths allow for separation of electromagnetic and hadronic showers. Photomultiplier tubes (PMTs) [7] connected to the fibers convert detected light to electrical signals. Analog-to-digital converters (ADCs) digitize the signals, and the ADC output of each calorimeter channel is computed every 25 ns[1].

## 2. Characteristics of anomalous noise in HCAL sub-detectors

The CMS ECAL and HCAL occasionally record anomalous signals which can be misinterpreted as energy deposits[2], and it is essential to remove such anomalous signals so that they do not contribute to the measured energy attributed to collision events. Several sources of anomalous signals in HCAL have been observed (Figure 1). Electronics and detector noise observed in the

[1] These 25 ns intervals are later referred to as "time slices", or TS

[2] A description of the removal of ECAL anomalous noise can be found in Ref. [8]

HB and HE occurs randomly and at a constant rate, independent of the beam conditions. Beam induced anomalous signals are observed in signals recorded by the PMTs of the HF calorimeter.

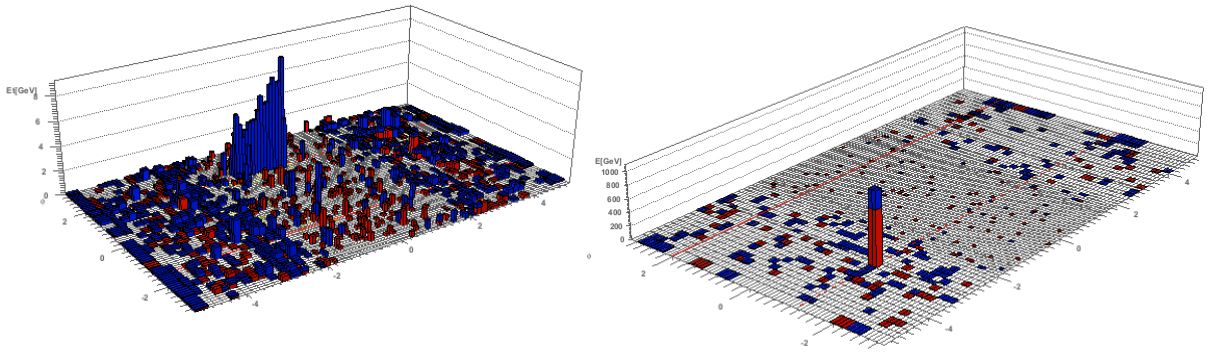

**Figure 1.** Event displays in $\eta$ and $\phi$ showing noise in HB (left), and in HF (right), in events overlapping with a $pp$ collision.

## 3. Identification of noise

Some of these anomalous noise signals were observed during past test beam and cosmic data taking [9], and detailed studies continued with the $pp$ collision data [10]. Two approaches are used in the treatment of noise overlapping with a collision event. In the first approach, the energy reconstructed in channels having anomalous signals is removed during event processing, so that the affected channels do not contribute to the reconstructed physics objects ("noise cleaning"). In the second approach, if many channels are identified as having noise, the entire event is discarded from the analysis ("noise filtering").

### *3.1. Noise in barrel in endcap*

Three categories of noise in HB and HE have been observed during both cosmic and collision data taking. Large signals are occasionally observed in the HPDs even when no light is incident on the photo-cathodes. These signals are originated by thermally emitted electrons which ionize the gas or surface molecules in the acceleration gap of the HPD, which in turn are accelerated back to the cathode, liberating additional electrons. This type of noise is referred to as "ion feedback", and manifests itself as a significant energy deposit in a single channel. Misalignments between the electric field within an HPD and the external solenoid field can lower the flashover voltage of the HPD, leading to an avalanche of secondary electrons, producing large signals in up to 18 channels of the HPD ("HPD noise"). Electronics noise in RBX can produce signals in channels of multiple HPDs within the RBX, which can affect up to all 4HPDs ("RBX noise").

*3.1.1. Noise filtering in HB and HE* The event filter to identify and reject noise events is based on channel multiplicity, total number of zero ADC counts, and the RBX "pulse shape ratio" ("R45"). An event is flagged as noise if any of the following conditions are met:

- at least 17 channels within an HPD with $E(\text{channel}) \geq 1.5$ GeV, or
- at least 10 channels within an HPD with $E(\text{channel}) \geq 1.5$ GeV, and there is no energy reported in the other HPDs contained in the same RBX, or

- at least 10 TSs within an RBX with zero ADC counts, and $E(\text{RBX}) \geq 10$ GeV.

The R45 variable is defined as R45=(E4-E5)/(E4+E5), where E4 and E5 are the energies measured in channels of that RBX, in the triggered and subsequent TSs, respectively. For real signals $\sim$ 90% of energy is contained within these two TSs, while noise pulses are generally broader. As can be seen from Figure 2, for events collected using a Minimum Bias trigger, majority of RBXs have the R45 distribution contained within the red *envelope*. The envelope defines the position of an energy dependent cut on the R45 variable: events with an RBX that has R45 above the upper curve, or below the lower curve are flagged as noise events.

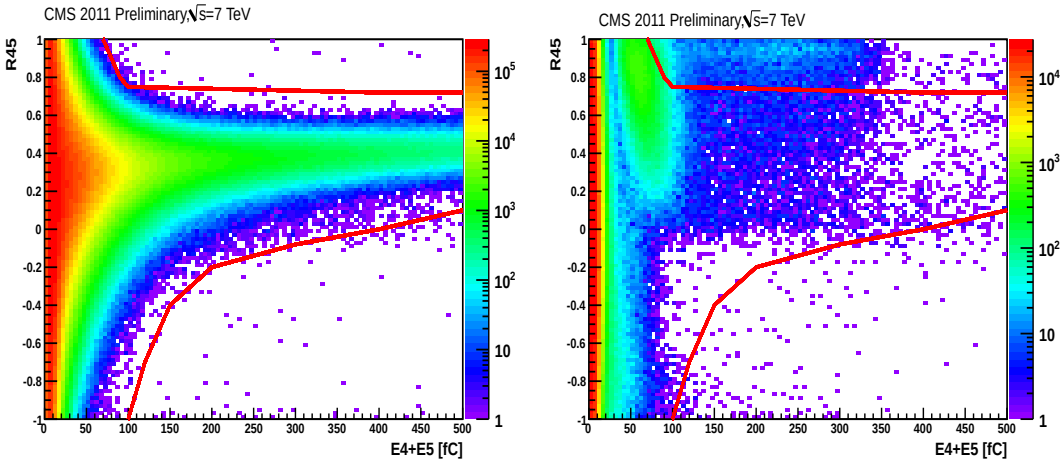


**Figure 2.** The distribution of R45 versus energy in E4+E5 for all RBXs in collision events (left), and events collected during periods with no circulating beams in LHC (right).

Events that fail any of the requirements listed above are marked as noise candidates, and discarded from physics analysis. The efficiency of the noise filter was measured in collision events, and was found to be >70-75%, with a misidentification rate of less than 0.3%. A modification of this filter that includes information from ECAL and tracker, and adds HCAL topological isolation requirements increases the efficiency to $> 95\%$, with misidentification rate $< 0.4\%$.

*3.1.2. Noise cleaning in HB and HE* A set of algorithms has been developed to further exploit the differences between noise and signal pulse shapes. The information used by these algorithms is largely uncorrelated to those described in Sec. 3.1.1, hence they provide additional identification power. In the fit-based algorithms a comparison of the measured and the ideal signal pulse shape is made, and a compatibility test to signal and noise hypothesis is performed. Two noise types are tested against the signal pulse, and the corresponding pulse-shapes are shown in Figure 3.

The linear discriminant is formed by comparing the $\chi^2$ from signal and noise shapes hypotheses fits. The noise hypothesis here is that the noise pulse shape is a linear function of the TS index (middle in Figure 3). A log ratio of the $\chi^2$ of the two hypotheses is then used as a discriminant variable to identify a channel as noisy. Another type of anomalous signals in HB and HE has the characteristics of all the charge being concentrated in one or two time slices, with very little activity in the remaining 8 TSs (right in Figure 3). "RMS8" is defined as the RMS value (in units of charge) of the lowest 8 TSs, divided by the maximum charge in all 10 TSs. The discriminant for this type of noise is then defined as the log ratio between the $\text{RMS8}^2$ and the $\chi^2$ to the ideal pulse shape. An energy dependent cut is then chosen for both of these algorithms using events collected during runs with no circulating beams in LHC.

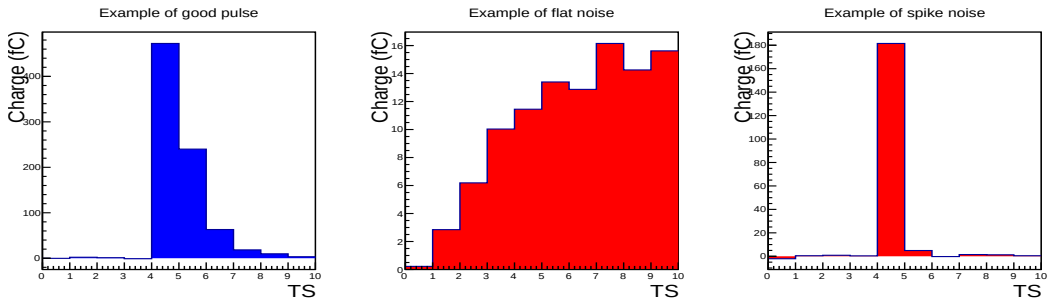


**Figure 3.** Pulse shapes of a good signal from hadronic shower (left) compared to common noise signals (middle and right). The events with noise pulses are collected during periods when there are no collisions in CMS.

The left plot Figure 4 shows a comparison of missing transverse (MET) energy reconstructed from channels only in HB and HE, before and after the noise cleaning is applied. As can be seen, the mis-identification rate is very low (below 0.01%). The middle plot in Figure 4 shows the distribution of energies of the noise signals identified by the fit-based algorithms, before applying the noise filter (Section 3.1.1). The right plot in Figure 4 shows the same distribution after the events identified by filter were rejected, showing the complementarity of the two algorithms.

*3.2. Noise in HF*

Anomalous signals in HF occur when particles interact in the HF PMT window, in the PMT device, or in the fibers. This type of noise is beam related and increases with increasing luminosity and is also $|\eta|$ dependent. PMT window events were first observed when HF modules were exposed to test beams, and the dominant source was found to be due to charged particles producing Čerenkov light in the thick glass window of the PMTs. A contribution is also observed from charged particles traversing the fiber bundle behind HF. Some of the high energy anomalous signals was found to originate from the material used to electrically isolate the PMT from the light guide ("sleeve"). This material produced scintillation light which was detected by the

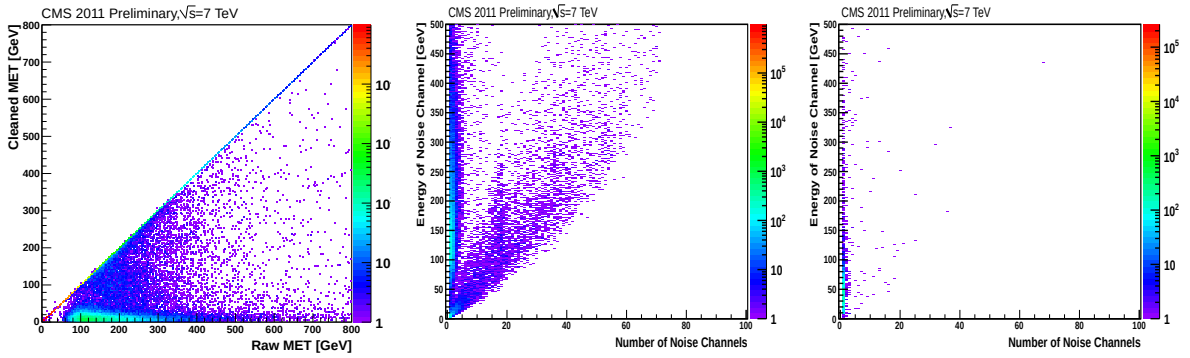


**Figure 4.** Comparison of MET computed using only HB and HE channels after cleaning (Y-axis) vs. after cleaning (X-axis) (left). Distribution of energies of the noise signals identified by the fit-based algorithms before applying the noise filter (middle), and the same plot after applying the noise filter (right). Events in all distributions are collected with a MET-based trigger.

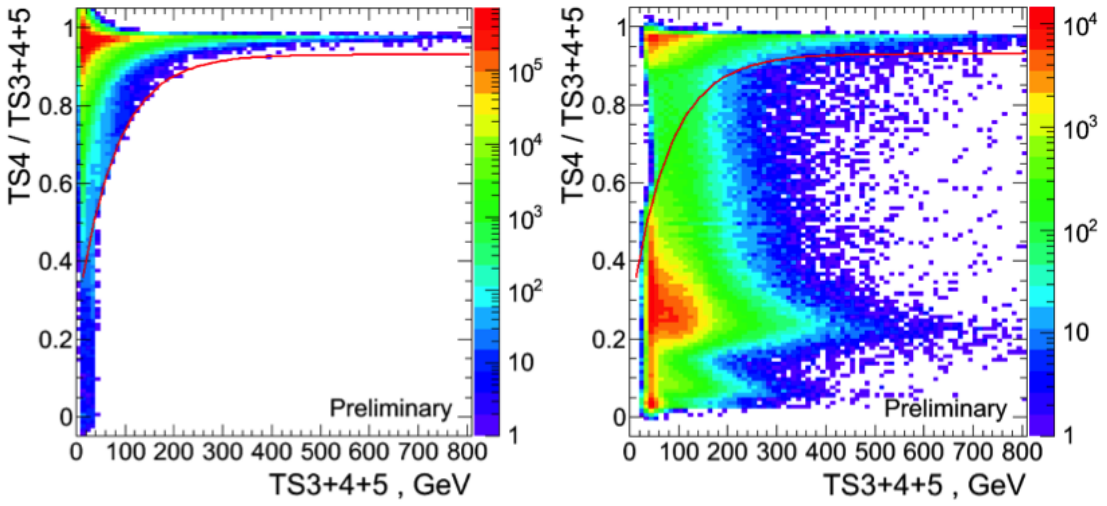


**Figure 5.** The distribution of PS1 ratio versus energy in TS3, 4 and 5, for all channels in HF in collision events (left), and events collected with a trigger based on jets in HF.

PMTs, and was replaced with a non-scintillating ones before 2011 data taking period.

The hits from relativistic charged particles impacting upon the PMT windows are subsequently detected and cause an early signal to be recorded for that individual channel. For relativistic particles the PMT window hits arrive significantly ahead of the Čerenkov light emitted in the HF absorber. The Čerenkov light captured by quartz fibers in the HF produces pulses having widths of only 10 ns. Therefore, the phase of HF electronics is setup so that the majority of the PMT window hits arrive in the TS previous to the triggering one, thus reducing the effect of noise on energy reconstruction.

*3.2.1. Pulse-shape cleaning in HF* The pulse shape based noise algorithm makes use of the ratio of energy $E$ recorded in the triggered TS (E4) to the energy in the TSs around it ($\Sigma E = E3 + E4 + E5$). A discriminator, referred to as PS1, is defined as PS1=E4/$\Sigma E$. True signal hits are expected to have a PS1 value near one. As can be seen from Figure 5, for events collected using a Minimum Bias trigger, majority of hits have the PS1 distribution contained within the red *envelope*. The envelope defines the position of an energy dependent cut on the PS1, and channels that have PS1 below the red curve are flagged as noise events.

*3.2.2. Topological cleaning in HF* Topological cleaning of noise in HF is performed on all channels which are not flagged as noise by the pulse shape algorithm. Three different algorithms are used, referred to as the "long-short" ratio, S8S1, and S9S1 algorithms.

An asymmetric ratio ($R$) of the energy deposited in the long ($E^L$) and short ($E^S$) fibers for the same channel, is defined as $R = |E^L - E^S|/(E^L + E^S)$. The $R$ ratio is computed for all channels, and checked whether it is greater than 0.8. If a channel's $R$ value is greater than 0.8 and its energy is greater than an $|\eta|$-dependent threshold, then the channel is marked as noise.

Two isolation-based variables are formed to account for the lateral profile of real showers:

$$S8S1 = \frac{\sum_{i=1}^{4} E_i^L + \sum_{i=1}^{4} E_i^S}{E}, \; S9S1 = \frac{E^S + \sum_{i=1}^{4} E_i^L + \sum_{i=1}^{4} E_i^S}{E^L} \qquad (1)$$

where the index $i$ runs over each channels adjacent cells. Any channel previously flagged as noise by the pulse shape filter or the PET algorithm is excluded from the construction of the

S8S1 or S9S1 variable. The S9S1 and S8S1 algorithms are applied to all channels with energy above 100 GeV, and energy dependent cut position is optimized on a sample of noise data. If the channel fails the cut, it's marked then the channel is marked as noisy, and discarded from the event reconstruction. The *S8S1* algorithm is applied to all short fiber hits , while the S9S1 algorithm is applied to all long fiber hits.

*3.2.3. Pre-triggering from noise in HF* Some of the noise in HF generate pulses that are reconstructed as early arriving signals. While this feature is exploited in rejecting the energies of such signals in event reconstruction, it can cause the trigger system to prematurely issue an "accept" signal, reading out the information from sub-detectors 25 ns earlier than the collision. An algorithm is implemented at the Level 1 trigger level, which vetos triggering in "BX-1", where BX is the colliding bunch crossing number. The BX number where proton bunches collide is identified using the Button Beam Pickup (BPTX) system [1]. The BPTX provides an accurate information on the timing and phase of each proton bunch, allowing one to calculate the interaction-point position from the relative phases of BPTX measurements on opposite sides of CMS. The "BX-1" veto was implemented in 2011 running, and was found to be fully effective in removing pre-triggers. Since *pp* collisions occur every 50 ns during the 2011-2012 running of the LHC, the BX-1 veto does not introduce any inefficiency at the trigger. The PMTs will be replaced during 2013-2014 LHC shutdown with thinner window PMTs that will significantly reduce the noise rates, and provide additional noise rejection due to multi-anode readout. This change will allow running with 25 ns bunch spacing without the BX-1 veto.

## 4. Summary

Several identification algorithms have been developed to suppress anomalous signals in CMS HCAL. The flexible software infrastructure allows to employ these algorithms both at the trigger level, and during the event reconstruction. The algorithms identify noise signals by exploiting the differences in pulse shape and energy isolation. It was shown that the efficiency in rejecting noise signals for high instantaneous luminosity of LHC data-taking in 2012 remains high.

This project was carried out with financial support from U.S. Department of Energy, U.S. National Science Foundation, RMKI-KFKI (Hungary), Russian Ministry of Education and Science, Russian State Committee for Atomic Energy, Scientific and Technical Research Council of Turkey (TUBITAK), Turkish Atomic Energy Agency (TAEK) and Bogazici University Research Fund.

## References

[1] S. Chatrchyan *et al.*, "The CMS experiment at the CERN LHC," *JINST* **3**, S08004 (2008)
[2] S. Chatrchyan *et al.*, "The CMS hadron calorimeter project: Technical Design Report", CERN-LHCC-97-031
[3] S. Abdullin *et al.*, "Design, Performance, and Calibration of CMS Hadron-Barrel Calorimeter Wedges", *Eur. Phys. J.* C **55** (2008).
[4] S. Abdullin *et al.*, "Design, Performance and Calibration of the CMS Forward Calorimeter Wedges", *Eur. Phys. J.* C **53** (2008).
[5] G. Baiatian *et al.*, "Energy Response and Longitudinal Shower Profiles Measured in CMS HCAL and Comparison With Geant4," CERN-CMS-NOTE-2006-143.
[6] P. Cushman, A. Heering, A. Ronzhin, "Custom HPD readout for the CMS HCAL", *Nucl. Instrum. Methods* A **442** (2000).
[7] U. Akgun *et al.*, "Complete tests of 2000 Hamamatsu R7525HA phototubes for the CMS-HF Forward Calorimeter", *Nucl. Instrum. Methods* A **550** (2005).
[8] D.A. Petyt, "Mitigation of Anomalous APD signals in the CMS Electromagnetic Calorimeter", Contribution to this conference.
[9] S. Chatrchyan *et al.*, "Identification and filtering of uncharacteristic noise in the CMS hadron calorimeter", *JINST* **5** T03014 (2010).
[10] S. Chatrchyan *et al.*, "Missing transverse energy performance of the CMS detector", *JINST* **6** P09001 (2011).